ンに記載されているものを表３，表４に示します。しかし，ガイドラインに示される術後早期の定期検査はすべてのステージの患者さんに対して３カ月ごとの血液検査を推奨するなど均一かつ頻回であり，最適なフォローアップ法とは言い難く，今後の検討課題です。

表３　転移・再発の危険性の比較的低いステージⅠ，Ⅱのフォローアップ

術後～２年半までの定期検査	３カ月ごと	理学検査，血液検査
	６カ月ごと	胸部レントゲン写真，腹部超音波検査または CT 直腸指診（直腸がん）
	１年ごと	骨盤 CT または MRI（直腸がん）
術後２年半～５年までの定期検査	６カ月ごと	理学検査，血液検査
	１年ごと	胸部レントゲン写真，腹部 CT

（大腸癌治療ガイドラインより）

表４　転移・再発の危険性の比較的高いステージⅢのフォローアップ

術後～３年までの定期検査	３カ月ごと	理学検査，血液検査
	６カ月ごと	胸部レントゲン写真，腹部超音波検査または CT 直腸指診（直腸がん）
	１年ごと	骨盤 CT または MRI（直腸がん）
術後３～５年までの定期検査	６カ月ごと	理学検査，血液検査，胸部レントゲン写真，腹部超音波検査または CT
	１年ごと	骨盤 CT または MRI（直腸がん）

（大腸癌治療ガイドラインより）

転移・再発の 97 ～ 98%は術後５年以内におこるため，フォローアップの期間は通常は術後５年間とされています。しかし，この期間の定期検査はあくまでも転移・再発の発見を第一の目的としており，他の臓器のがん（胃がんや子宮がんなど）の早期発見には向かないこと，術後５年以降に大腸の他部位にあらたにがんが発生する場合もあることなどを忘れてはいけません。担当医と相談し，職場や市町村で適切な検診を受けることをお勧めします。

現在，多施設の共同研究で術後の再発部位や確率を考慮した最適のフォローアップの方法，期間の研究が行われています。

（上原圭介・山本聖一郎・森谷宜皓）

子宮がん、膀胱がん、
直腸がん等の骨盤内腫瘍

進行・再発骨盤腫瘍に対する骨盤内灌流化学療法

◆50回分の全身化学療法に匹敵する治療効果。副作用は最小限の半分以下に

子宮や膀胱、直腸など骨盤の中に存在する臓器を骨盤内臓器というが、その骨盤内臓器に発生したり、そこへ転移してきたりした進行・再発骨盤内腫瘍を治癒させる画期的治療法が登場した。骨盤の中だけで血液を循環させ、一定時間、腫瘍を抗がん剤漬けにする骨盤内灌流化学療法がそれだ。

骨盤内の人工循環システムに大量の抗がん剤を投与

抗がん剤を大量に投与すればがんは死滅するが、副作用も大きいので患者は耐えられない。かといって、患者が耐えられる程度の投与量にとどめれば、がんの死滅ははかれない。抗がん剤治療に伴うこの不可避なジレンマを突き破る画期的な治療法が骨盤内灌流化学療法だ。

「骨盤内灌流化学療法は子宮や膀胱、直腸等の骨盤内臓器から発生した原発がん（子宮がん・膀胱がん・直腸がん等）と、他臓器から転移してきた骨盤内腫瘍が治療の対象となります。骨盤へ通じる主要な血管を詰めて閉塞し、骨盤の中を一時的に隔離します。そのうえで人工心肺装置（ポンプ）で骨盤内の血流を循環させ、そこに抗がん剤を投与し、がんを死滅させようというのが骨盤内灌流化学療法です」

と日本医科大学附属病院の村田智講師（放射線科）は説明する。

骨盤に独立した循環システムがつくられ、腫瘍は一定時間（30分間）抗がん剤に曝露され続ける。その結果、抗がん剤を大量投与したときと同じように腫瘍内の抗がん剤濃度は高まり、強力にがんの死滅がはかられるのだ。

一方、骨盤の内外を繋ぐ主要血管はバルーン（風船）によって閉塞・遮断されるので、骨盤の外へ漏れ出る抗が

村田智講師
日本医科大学附属病院放射線科
〒113-8603
東京都文京区千駄木1-1-5
TEL 03-3822-2131
FAX 03-5685-1795

ん剤は少量にとどまる。ほんのわずかな抗がん剤しか全身へ漏出しないから、白血球の減少や吐き気、嘔吐等の副作用は最小限に抑えられ、先述した抗がん剤治療のジレンマを克服することができるのである。

瀬川泰子さん（48歳）が子宮頸がんと診断されたのは2004年の4月。腫瘍の大きさは長径5㎝近くに及び、子宮周囲の組織やリンパ節に広く浸潤し、ステージⅢb期の進行がんと診断された。

瀬川さんの進行子宮頸がんは、手術で腫瘍を切除しきれないことから、通常は放射線と抗がん剤による放射線併用化学療法で治療する。しかし、半数以上の患者が再発し、5年生存率は40％前後にとどまる。腫瘍が骨盤という身体の奥深いところに存在するため、確実にがんを死滅させる十分な放射線量がかけられない。加えて、副作用のため抗がん剤も不足のない量が投与できず、いずれも中途半端な治療となることが少なくないからである。

幸いなことに瀬川さんは腫瘍の広がりが骨盤内にとどまっていたことから、村田講師の骨盤内灌流化学療法を受けた。

最初の治療でかなり縮小したものの、まだ腫瘍が残っていたので2回目の治療を受けた。結局、計3回の治療で腫瘍のすべてが跡形もなく消失し、CT等の画像検査と生検でそれが確認された。

「骨盤内灌流化学療法でもたらされる腫瘍内の抗がん剤濃度は、通常の静脈から点滴投与する全身化学療法の50倍に達します。いわば、1回の骨盤内灌流化学療法は50回分の全身化学療法に相当するため、骨盤の中に広がる子宮頸がんでも確実に消失させることができたのです」（村田講師）

驚くのは抗がん剤の副作用にほとんど苦しまなかったことだ。瀬川さんは骨盤内灌流化学療法を受けた当日だけ少し吐き気を覚えたが、翌日からもう副作用とは無縁の生活に戻ることができた。

「骨盤内灌流化学療法は抗がん剤による副作用やダメージが最小限に抑えられるので、がん患者にとって優しい治療といえるのです」（村田講師）

骨盤内灌流化学療法が効くのは、手術不能の進行がんだけではない。骨盤内に腫瘍が再発した場合も、がんが骨盤内にとどまっている限り、がんの消失＝治癒が得られる可能性は大きい。

治癒が得られないケースでも、腫瘍の大幅な縮小から症状の改善や生活の質（QOL）の向上、生存期間の延長がはかられるため、がん患者とその家族から熱い期待が寄せられている。

腫瘍内の抗がん剤濃度は全身化学療法の50倍に

骨盤内腫瘍は左右の寛骨（腸骨・坐骨・恥骨の三つが一体となった骨）と仙骨、尾骨から構成される骨盤内の臓器から発生したり、骨盤内へ転移してきたがんだ。

「身体の深部にできるため、進行してから発見されることが少なくありません。周辺に広く浸潤し、手術でがんのすべてを切除するのは難しい。周辺の重要臓器に障害をもたらしかねない放射線治療や、十分な量を投与するのが難しい抗がん剤治療も躊躇せざるを得ません」（村田講師）

加えて、骨盤の中は排尿・排便等を司る神経や細かな血管が縦横に走り、重要臓器やリンパ節なども数多い。治療が功を奏し治癒しても、しばしば排尿・排便障害やリンパ浮腫などに悩まされる。がんが残存し再発を招いたときは、増殖するがんによって痛みが増大したり、腸閉塞など不測の事態を招き、急速に症状の悪化とＱＯＬの低下を招いて死期を早めかねない。

「いずれにせよ進行・再発骨盤内腫瘍は、従来の手術や放射線、抗がん剤による治療では難渋せざるを得ません。根治が得られると同時に、臓器や機能も温存できるという一挙両得な革新的治療法が切実に求められてきました。骨盤内灌流化学療法はそうしたがん患者さんとその家族の願いに応える新たな治療法といえるでしょう」（村田講師）

周知のように、抗がん剤の治療効果は腫瘍内の抗がん剤濃度と相関し、それを高めるほどがん細胞の死滅がはかられる。しかし、従来の静脈から点滴投与する全身化学療法では、腫瘍へ到達する抗がん剤の量はかなり目減りせざるを得ない。しかも、抗がん剤の副作用は全身に現れるから、それに耐えられる許容範囲が投与量の上限となる。

「腫瘍内の抗がん剤血中濃度を上げるには、全身化学療法はあらかじめ厳しい足枷をはめられている治療法なのです」（村田講師）

一方、腫瘍の間近までカテーテルを挿入し、腫瘍へ直接抗がん剤を投与する動脈内抗がん剤注入療法（動注）は、たしかに全身化学療法より多量の抗がん剤を腫瘍に送りこめる。しかし、腫瘍内の抗がん剤濃度が上昇するのは、抗がん剤を注入した直後のみだ。一過性にすぎず、腫瘍内抗がん剤濃度は再び低下せざるを得ない。注入された抗がん剤は静脈から全身に流れて循環することから、結局、全身化学療法以上の大量の抗がん剤を投与することはできない。

ところが、骨盤内灌流化学療法は一

時的に骨盤を隔離した独立環境に置き、その中に設けられた閉鎖循環システムに通常の2倍の抗がん剤を投与し、それを30分間にわたって連続的に循環させる。（図）

「抗がん剤を効果的かつ集中的に腫瘍へ送りこむ新たなドラッグ・デリバリー・システム（ＤＤＳ＝薬物送達システム）に基づく化学療法です。いわば、骨盤内腫瘍を一定時間抗がん剤漬けの状態にしますから、腫瘍内の抗がん剤濃度は飛躍的に高められます。全身化学療法と比べ、腫瘍内濃度を50倍に上げられるのは驚異的といえます」（村田講師）

しかも、骨盤の中から全身に漏れ出る抗がん剤は20％程度にとどめられ、全身に回る抗がん剤は全身化学療法を行った場合に漏れ出る量の約40％にすぎない。当然、抗がん剤の副作用に苦しむことはほとんどない。骨盤内灌流化学療法が、難渋する骨盤内腫瘍の決め手として大きな注目を集めているゆえんである。

バルーンカテーテル等で血流を遮断した骨盤内灌流システム

骨盤内灌流化学療法はまず全身麻酔をかけ、左右の太股の付け根（鼠蹊部）を小切開し、大腿動脈と大腿静脈へカテーテル挿入器（シース）を差し入れる。

図を参考に説明すると、次にバルーンカテーテルを大腿動脈のシースから挿入し、外腸骨動脈から総腸骨動脈へ進入させ、その先端が腹部大動脈へ少し入ったところで、カテーテルの先端に付いているバルーン（風船）を膨らませて血流を止める。

「一方、もう1本のバルーンカテーテルを大腿静脈のシースに挿入し、同じようにその先端が下大静脈へ少し入ったところでバルーンを膨らませて血流を遮断します」（村田講師）

次に太股をベルト（タニケット）で圧迫し、足先への血流を止めると、基本的に骨盤の中の血流は隔離される。

もちろん骨盤の内外を結ぶ大小の血管（側副血行路）はほかにも存在するから、必要があれば側副血行路を丁寧にコイル等を用いて遮断する。

骨盤の中の血流を隔離したら、左右の大腿動脈と大腿静脈に差し入れたシースと人工心肺装置（ポンプ）、人工透析装置をチューブで繋ぎ、抗がん剤の灌流システムを構築する。大腿動脈へ差し入れたシースから抗がん剤を投与し、骨盤内へ抗がん剤を注入する。

「一方、大腿静脈へ差し入れたシースから抗がん剤を含んだ血液がポンプで吸入され、再び大腿動脈に差し入れたシースから骨盤内に送りこまれるので

す」（村田講師）

抗がん剤はシスプラチン等のプラチナ製剤を主体に投与する。プラチナ製剤は腫瘍内の抗がん剤血中濃度とがん細胞に対する殺傷力が、きわめてよく相関するからだ。

「子宮頸がんの場合はシスプラチンのみです。膀胱がんはシスプラチンにマイトマイシンCを加えます。個々の腫瘍ごとに、適宜、もっとも有効な抗がん剤を追加します」（村田講師）

抗がん剤は10分ごとに2～3回投与し、30分間循環させる。その間、腫瘍内の抗がん剤濃度が、全身化学療法の50倍に上昇することは先述した通りである。

循環させた後はただちに人工透析装置を稼働させ、骨盤内を隔離したまま血液中から抗がん剤を濾過する。血液中の抗がん剤は1時間の血液透析でほぼすべて除去される。手術室で全身麻酔をかけられてから、約3時間で骨盤内灌流化学療法は終了する。

最初の骨盤内灌流化学療法で腫瘍が消失しないときは、4週間後に2回目を行う。その後は治療効果と患者の状態を見ながら、繰り返すか否かを適切に判断していく。

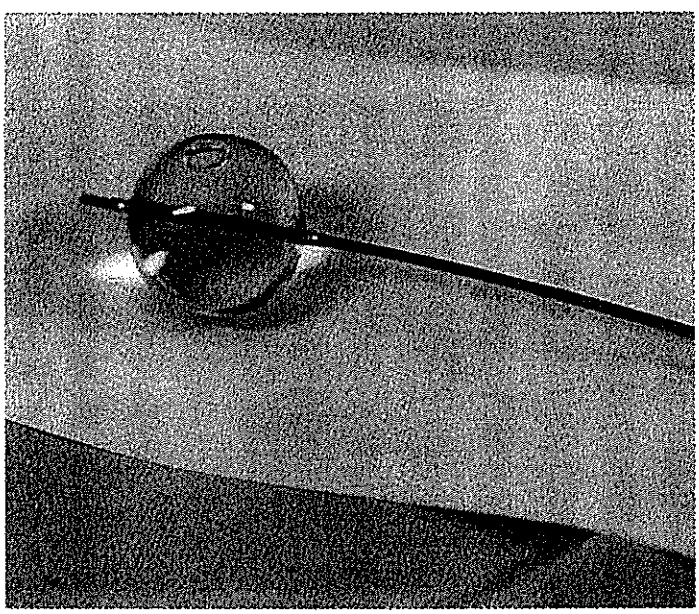

進行、再発がんでも骨盤内の腫瘍なら、一挙に叩き根治を狙える

骨盤内灌流化学療法の優れた治療効果は、たしかな治療成績によって立証されている。

「一番効果が期待できるのは子宮頸がんと膀胱がんです。骨盤内に腫瘍がとどまっている子宮頸がんや膀胱がんは、どんなに進行・再発していても骨盤内灌流化学療法によって根治が狙えます」（村田講師）

子宮頸がんは通常、子宮頸に沿って子宮体部と膣の方向へ浸潤し、さらに子宮を骨盤につなぎとめている子宮傍結合組織へ広がる一方、リンパ液の流れに乗ったがん細胞が骨盤内リンパ節へ転移する。そんなに広がっていない早期がんのうちなら手術による切除も可能だが、広範囲に広がる進行・再発がんに放射線療法や化学療法を加えて

【骨盤内灌流化学療法の閉鎖循環システム】

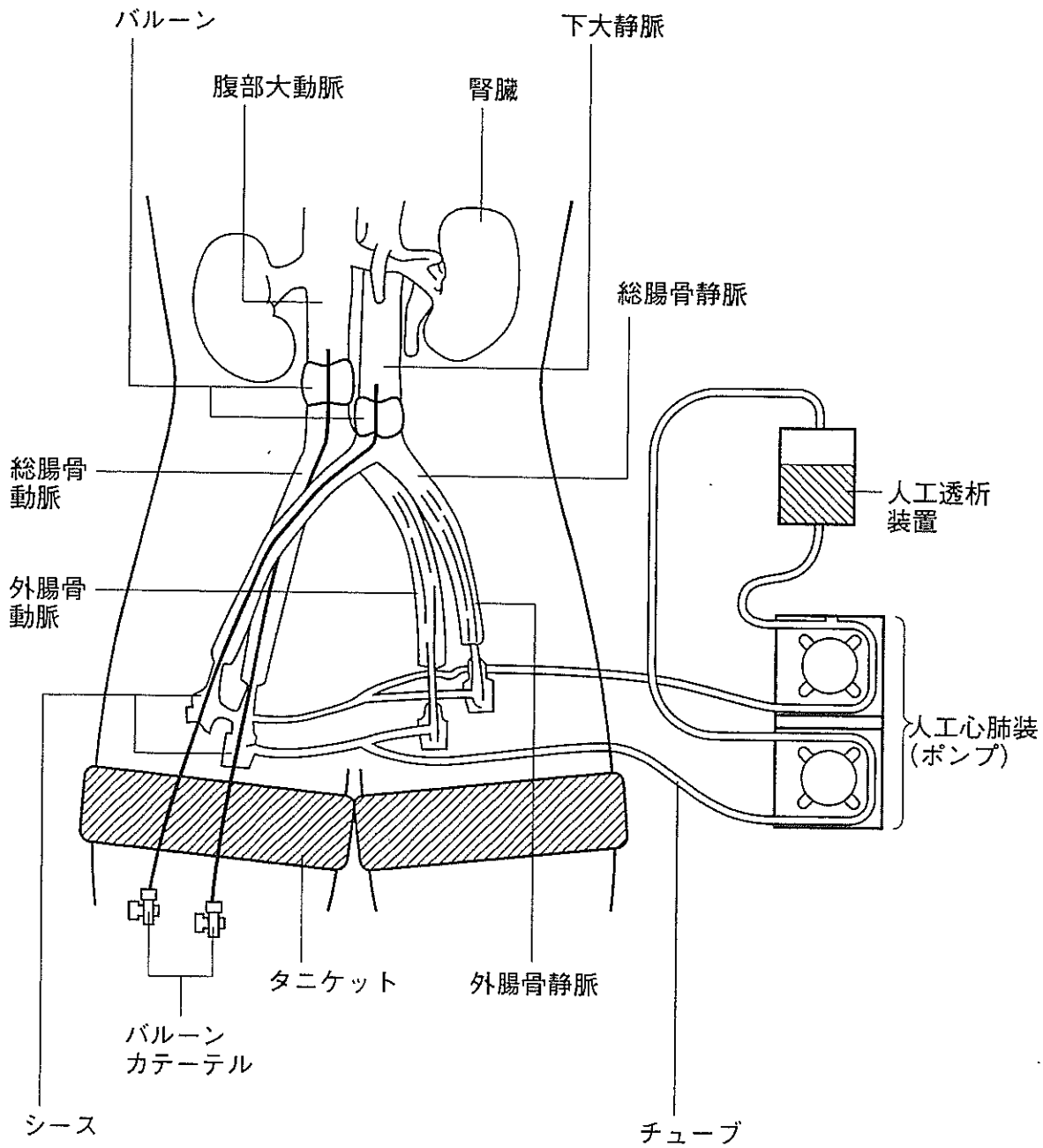

骨盤内灌流化学療法では太ももの付け根を小切開し、大腿動脈と大腿静脈へカテーテル挿入器（シーズ）を挿し入れ、そこへバルーンカテーテルを挿入し外腸骨動脈から総腸骨動脈へ進入させ、その先端が腹部大動脈へ入ったところでバルーンを膨らませて血流を止める。一方、もう１本のバルーンカテーテルを同じように大腿静脈から外腸骨静脈、総腸骨静脈へ進入させ、下大静脈へ少し入ったところでバルーンを膨らませる。次に、太ももをベルト（タニケット）で圧迫して足先への血流を止めると、骨盤内の血流は基本的に隔離されて閉鎖循環システムが構築される。

もがん細胞は残存し治癒させるのが難しい。しかし、骨盤の中で抗がん剤を循環させる骨盤内灌流化学療法は、進行・再発巣やリンパ節転移などすべての腫瘍を洗い流すように、一挙に叩き死滅させることから根治が得られるのである。

膀胱がんは浸潤性膀胱がんが対象となる。腫瘍が膀胱壁の筋層より深く浸潤しているものの、骨盤内にとどまる進行膀胱がんだ。通常は手術で膀胱を全摘するが、5年生存率は25～53％で、かならずしも治療成績がいいとはいえない。加えて、膀胱の全摘によって自然な排尿ができなくなり、ＱＯＬの低下も免れない。しかし、骨盤内にとどまる浸潤性膀胱がんならば、骨盤内灌流化学療法で確実に治癒へ導けると同時に、膀胱を温存することで自然な排尿も可能となる。

「重要なのはがんの消失が得られない場合でも、骨盤内灌流化学療法で腫瘍の縮小をはかり、すみやかな症状の改善やＱＯＬの向上、生存期間の延長などがかちとれることです」（村田講師）

直腸がんや子宮体がん等が進行・再発すると、腫瘍の増大から痛みや腸閉塞、排尿・排便障害などさまざまな症状が噴出する。モルヒネの増量や対症療法的手術、放射線照射などさまざまな方法で治療するものの、しばしば錯綜する症状の前に有効な手を打てなくなるが、骨盤内灌流化学療法によって強力に腫瘍が縮小し、すみやかな症状の軽減をはかれるのである。

「骨盤内灌流化学療法は1999年からはじめ、これまでに70人前後の患者さんに試みてきましたが、腫瘍が消失した患者さんも少なくありません。加えて、腫瘍が消失しないまでも縮小したり、発育が止まったりした患者さんを含めると奏効率はほぼ100％近くにのぼります」（村田講師）

「骨盤内悪性腫瘍に対する閉鎖循環下における抗がん剤灌流療法（ＮＩＰＰ）」というのが、骨盤内灌流化学療法の正式な名称である。欧米の類似した治療法を参考に、先の村田講師がその欠陥を補って新たに確立したものだ。2004年に厚生労働省「がん治療のための革新的新技術の開発」班（第3次厚労省厚生科学研究費がん克服研究事業）の研究課題としてとりあげられたのは、非常に有望な治療法と認められたからだ。

現在、骨盤内灌流化学療法は日本医大附属病院（放射線科）のほかに、琉球大学医学部附属病院（放射線科）や海老名総合病院（放射線科）でも行われている。骨盤内腫瘍の治療に難渋するがん患者とその家族にとって、骨盤内灌流化学療法は大きな希望の光といってよいだろう。早急な普及が強く望

まれる。

同様の治療法を行っている他の主な医療機関

◆海老名総合病院放射線科
渡潤部長
TEL046・233・1311

◆琉球大学医学部附属病院放射線科
宜保昌樹医師
TEL098・895・3331

Dose-volume delivery guided proton therapy using beam on-line PET system

Teiji Nishio[a] and Takashi Ogino
Particle Therapy Division, Research Center for Innovative Oncology, National Cancer Center, Kashiwa, 6-5-1 Kashiwano-ha, Kashiwa-shi, Chiba 277-8577, Japan

Kazuhiro Nomura
Director, National Cancer Center Hospital, 5-5-1 Tsukiji, Chyuou-ku, Tokyo 104-0045, Japan

Hiroshi Uchida
The 5th Research Group, Hamamatsu Photonics K. K., 5000 Hirakuchi, Hamakita-shi, Shizuoka 434-8601, Japan

(Received 6 February 2006; revised 14 September 2006; accepted for publication 15 September 2006; published 19 October 2006)

Proton therapy is one form of radiotherapy in which the irradiation can be concentrated on a tumor using a scanned or modulated Bragg peak. Therefore, it is very important to evaluate the proton-irradiated volume accurately. The proton-irradiated volume can be confirmed by detection of pair annihilation gamma rays from positron emitter nuclei generated by the target nuclear fragment reaction of irradiated proton nuclei and nuclei in the irradiation target using a positron emission tomography (PET) apparatus, and dose-volume delivery guided proton therapy (DGPT) can thereby be achieved using PET images. In the proton treatment room, a beam ON-LINE PET system (BOLPs) was constructed so that a PET apparatus of the planar-type with a high spatial resolution of about 2 mm was mounted with the field of view covering the isocenter of the beam irradiation system. The position and intensity of activity were measured using the BOLPs immediately after the proton irradiation of a gelatinous water target containing ^{16}O nuclei at different proton irradiation energy levels. The change of the activity-distribution range against the change of the physical range was observed within 2 mm. The experiments of proton irradiation to a rabbit and the imaging of the activity were performed. In addition, the proton beam energy used to irradiate the rabbit was changed. When the beam condition was changed, the difference between the two images acquired from the measurement of the BOLPs was confirmed to clearly identify the proton-irradiated volume. © *2006 American Association of Physicists in Medicine.* [DOI: 10.1118/1.2361079]

Key words: dose-volume delivery guided proton therapy (DGPT), beam on-line PET system (BOLPs), target nuclear fragment reaction

I. INTRODUCTION

Recently, the use of proton therapy, which is a highly accurate type of radiotherapy, has been spreading throughout the world. The construction of proton therapy facilities is now progressing in many countries, including the United States and countries in Europe and Asia.[1] In conformal radiotherapy, image guided radiation therapy (IGRT) is a highly accurate method of radiotherapy that can precisely irradiate the tumor by navigation of radiation to be delivered based on images such as CT images and ultrasound images.[2,3] As a result, a high dose of radiation to a tumor may be delivered.

In proton therapy, the depth dose distribution has a Bragg peak. Because of the typical proximity of the proton beam to critical structures, it is beneficial to examine the proton irradiated volume and dose distribution during treatment.

Dose-volume delivery guided proton therapy (DGPT) is achieved by navigating the activity image of the distribution and intensity of the positron emitter nuclei generated by the target nuclear fragment reaction of irradiated proton nuclei and other nuclei in the patient.[4–6] A beam on-line positron emission tomography (PET) system (BOLPs), which has a high position resolution, has been developed and constructed with the field of view covering the isocenter of the beam irradiation system in the proton treatment room for DGPT.

The activities of the positron emitter nuclei generated by the target fragmentation nuclear reaction in a gelatinous water target and a frozen rabbit were measured at several proton energy levels using the BOLPs. The change between the proton dose distribution and the activity distribution of the generated positron emitter nuclei was confirmed and verified.

This report is organized as follows: The performance of the BOLPs, experimental setup and procedures are described in Sec. II. Measurement and analysis results are presented in Sec. III. Finally, Sec. IV discusses the conclusions made, based on the results, the usefulness of the BOLPs, and the plans for future developments.

II. MATERIALS AND METHODS

A. Generation of positron emitter nuclei in the target

Many kinds of nuclei, including positron emitter nuclei, are generated by the target nuclear fragment reaction $X(p,x)Y$ of the irradiated proton nuclei and target nuclei in the patient.

The reaction cross section of $\sigma_{X\to Y}$ which determines the rate of generation, depends on the kind of target nucleus (mass number of A_t and atomic number of Z_t) and relative kinetic energy of E_p. The number of nuclei generated by the reaction N_R is expressed as follows:

$$N_R(T_i,N_p,\sigma_{X\to Y}) = N_p(T_i,E_p)\cdot[1-\exp(-\sigma_{X\to Y}(A_t,Z_t,E_p)\cdot n(A_t,Z_t)\cdot\delta(A_t,Z_t))]. \quad (1)$$

Here, T_i denotes the time of the proton irradiation, n is the number of target nuclei per volume, and δ is thin thickness of the target. N_p is the number of incident protons of E_p in the irradiation of T_i at each position in the target. The residual number of positron emitter nuclei in the patient immediately after irradiation, N_{act}, depends on T_i, and is expressed using Eq. (1) and decay correction of the activity during the proton irradiation (refer to Appendix) as follows:[4]

$$\begin{aligned} &N_{\mathrm{act}}(T_i,T_{1/2},N_p,\sigma_{X\to Y}) \\ &=\sum_Y\left\{N_R(T_i,N_p,\sigma_{X\to Y})\cdot\left[\frac{T_{1/2}}{T_i\cdot\ln 2}\cdot(1-2^{-T_i/T_{1/2}})\right]\right\} \\ &=\sum_Y\left\{N_p(T_i,E_p)\cdot[1-\exp(-\sigma_{X\to Y}(A_t,Z_t,E_p)\cdot n(A_t,Z_t)\cdot\delta(A_t,Z_t))]\cdot\left[\frac{T_{1/2}}{T_i\cdot\ln 2}\cdot(1-2^{-T_i/T_{1/2}})\right]\right\}. \end{aligned} \quad (2)$$

Here, $T_{1/2}$ is the half-life time of the generated positron emitter nuclei.

The human body is composed mainly of the nuclei of the elements of H, C, N, and O.[7] Therefore, the positron emitter nuclei generated by the target nuclear fragment reaction are predicted to be mainly the ^{15}O [half-life time, $T_{1/2}(^{15}\mathrm{O})=122.2$ s], and ^{14}O [$T_{1/2}(^{14}\mathrm{O})=70.6$ s], ^{13}N [$T_{1/2}(^{13}\mathrm{N})=9.971$ min], ^{11}C [$T_{1/2}(^{11}\mathrm{C})=20.4$ min] nuclei. Moreover, the ^{38}K nucleus [$T_{1/2}(^{38}\mathrm{K})=7.6$ min] may be generated from the Ca nucleus in the bone.

B. Beam on-line PET system

The BOLPs is a system constructed for the determination of the position and the activity of the positron emitter nuclei by the detection of pair annihilation gamma rays from the nuclei. Two opposing detector heads of a planar positron imaging system (Hamamatsu Photonics K. K., Hamamatsu, Japan) mounted with BGO scintillators[8] are used for the BOLPs. Each detector head consists of 24 detector units, and each unit is composed of 10×10 arrays of BGO crystals with a crystal size of $2\times2\times20$ mm^3. The useful field size for the detection area is 120.8×186.8 mm^2. The BOLPs are mounted with a 500-mm distance between the upper and lower opposing detector heads and alignment of the center of the detection area at the isocenter in the rotating gantry treatment room of the proton therapy facility at our center.[9] The setup is shown in Fig. 1. The position resolution of this system is 1.6–2.1 mm for the full width at half maximum (FWHM) in the experiment using a ^{22}Na point source, and the collection rate of the data for the coincident detection of pair 511-keV gamma rays is over a few thousand counts per second (kcps).[8]

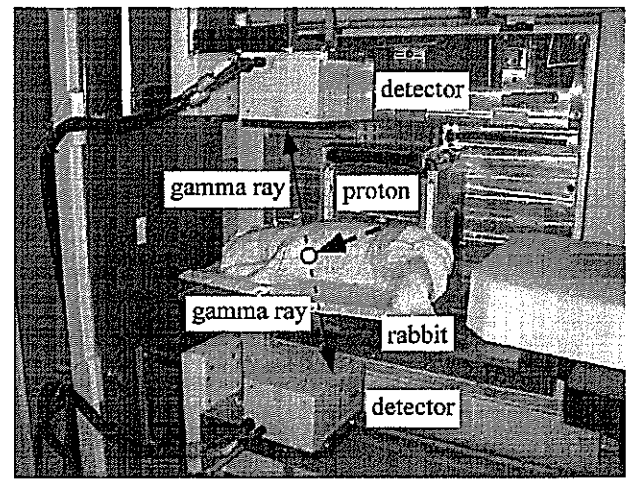

FIG. 1. Setup of the BOLPs on the proton beamline in the treatment room.

The activity measured by the BOLPs N_{BOLPs} is expressed using Eq. (2), decay correction of the activity during the measurement, and the total detection efficiency C_{eff} of the BOLPs as follows:

$$\begin{aligned} &N_{\mathrm{BOLPs}}(T_i,T_{1/2},T_m,N_p,\sigma_{X\to Y}) \\ &=N_{\mathrm{act}}(T_i,T_{1/2},N_p,\sigma_{X\to Y})\cdot[1-2^{-T_m/T_{1/2}}]\cdot\varepsilon^2\cdot\frac{\Omega_{\mathrm{sa}}}{4\cdot\pi} \\ &=\sum_Y\left\{N_p(T_i,E_p)\cdot[1-\exp(-\sigma_{X\to Y}(A_t,Z_t,E_p)\cdot n(A_t,Z_t)\cdot\delta(A_t,Z_t))]\cdot\left[\frac{T_{1/2}}{T_i\cdot\ln 2}\cdot(1-2^{-T_i/T_{1/2}})\right]\cdot[1-2^{-T_m/T_{1/2}}]\right\} \\ &\cdot\varepsilon^2\cdot\frac{\Omega_{\mathrm{sa}}}{4\cdot\pi}. \end{aligned} \quad (3)$$

Here, T_m denotes the time of the measurement after the proton irradiation, $\varepsilon(\approx0.86)$ the detection efficiency for a single 511-keV gamma ray, and Ω_{sa} the solid angle of the total detectors. The solid angle at each point is calculated with the adjoined detector unit. Therefore, C_{eff} of the BOLPs with a 500-mm distance between each opposing detector head is range of 0.3%–0.7%.

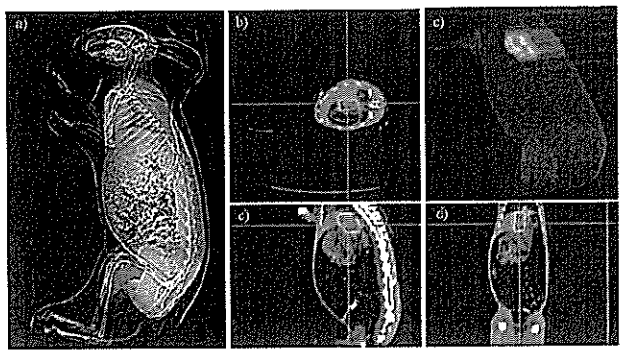

FIG. 2. Proton dose distribution in the liver of the rabbit calculated using the proton treatment planning system for plan 1 in the projection image (a), axial (b), sagittal (c), and coronal (d) planes in two dimensions and three dimensions (e), respectively.

C. Experimental procedures of proton irradiation to a water target

The proton beams used were monoenergetic Bragg peak (MONO) beams at 135.8 MeV and fine degraded energies in the short beam range of 0.6 mm WEL, 1.2 mm WEL, 2.3 mm WEL, 4.6 mm WEL, 9.3 mm WEL, and 18.6 mm WEL against the range of 135.8 MeV. The energies are 135.5 MeV, 135.1 MeV, 134.4 MeV, 133.0 MeV, 130.2 MeV, and 124.5 MeV, respectively. The MONO beam size was about 30 mm FWHM.

The target was gelatinous water (99% pure water), and had a rectangular shape of $10\times10\times40$ cm^3. The MONO beam of a very high intensity was directly irradiated to the water target for 5 s, and the irradiated dose was 6.5 Gy at the target entrance. The activity generated in the target was measured over a period of 33 min from the start of the proton irradiation using the BOLPs. Moreover, the 135.8-MeV MONO beams were irradiated to the target by the beam-irradiated position shifted with 1.0 mm, 2.0 mm, 4.0 mm, and 8.0 mm for a verification of the lateral distribution of the activity. The measurements of the lateral distribution were performed on the same condition as the measurements of the depth distribution.

The proton dose distributions were measured at intervals of 1 mm using a three-dimensional water phantom with a 75 μl farmer-type chamber, and compared with the distributions of the activity.

D. Experimental procedures of proton irradiation to a rabbit

The proton treatment of a patient was simulated using a frozen rabbit of about 60 cm total length. CT imaging, treatment planning, proton irradiation, and measurements using the BOLPs were performed using the same rabbit.

1. CT scanning

A frozen rabbit was wrapped with the fixed shell (ESFORM: Engineering System Ltd., Nagano, Japan) used for the proton treatment of the head and neck to maintain the shape of the rabbit and to mark for the positioning using a laser. Nonhelical CT imaging of 3-mm slices was performed with the x-ray tube at 120 kV and 200 mAs using a CT simulator (CT/Real+DR system, Toshiba Ltd., Tokyo, Japan). Views of the CT scanning instrument and the acquired projection image of the rabbit are shown in Fig. 2.

2. Proton treatment planning

The proton treatment planning system, PTPLAN/ndose, developed in our facility[10,11] was used for planning the proton treatment of the rabbit using the acquired CT image. A boot-shaped virtual tumor, which had a bend in the vicinity of the center and an 8.4-ml volume, was set in the liver of the rabbit. All of the gross target volumes (GTV), the clinical target volumes (CTV), and the planning target volumes (PTV) were set to be equal to the virtual tumor. The PTV (=CTV=GTV=virtual tumor) was irradiated with a dose of 4.0 Gy at the reference point with a single irradiation field from the backside at gantry angles=90° (plan 1). The maximum range of the irradiated proton beam in plan 1 was 82.4 mm WEL, and the energy was 103 MeV. The size of the irradiation field was 29 mm×54 mm, and the spread-out Bragg peak (SOBP) of 30 mm was used for the proton irradiation of the rabbit. The patient compensator and collimator were produced based on the results of the treatment planning. Moreover, another treatment plan was made assuming the partial reduction of the tumor size (plan 2). The maximum range was changed to 95.0 mm WEL in plan 2. The irradiated dose in plan 2 was 4.0 Gy at the reference point, which was the same as that in plan 1.

Figure 2 shows the proton dose distribution calculated using the proton treatment planning system in the axial, sagittal, and coronal planes in two dimensions, and in three dimensions for plan 1.

3. Proton irradiation

The proton irradiation was performed in the rotating gantry room at our facility. The positioning of the rabbit was performed by matching the marker on the fixed shell to the laser in the treatment room. A 4.0-Gy dose of the 103 MeV/SOBP30 mm proton beam at a 90° gantry angle was used to irradiate the PTV in the liver of the rabbit using the patient compensator and collimator produced in plans 1 and 2. The irradiated dose is generally daily fractional dose for a proton therapy of a liver and lung tumor in our facility. The proton irradiation time was about 1 min.

4. PET imaging using BOLPs

Figure 1 shows the setup of the rabbit and the BOLPs on the proton beamline. Both the center of the detection area in the BOLPs and the reference point in the PTV were matched up to the isocenter. In both plans 1 and 2, the activity generated in the liver of the rabbit was measured over a period of 33 min (beam on: 1 min, beam off: 32 min) from the start of the proton irradiation using the BOLPs. The measured data were stored in a computer for image display and for analysis of the binary formatted data pixels of 1.11-mm size

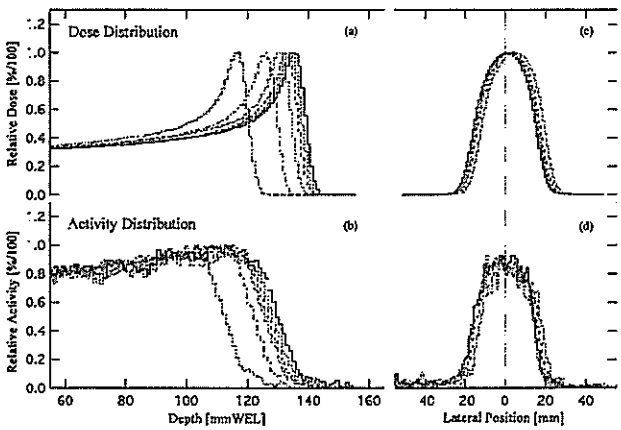

FIG. 3. Measured distributions of positron emitter nuclei generated in the water target and the measured dose distributions by irradiation of MONO proton beams at 135.8 MeV, 135.5 MeV, 135.1 MeV, 134.4 MeV, 133.0 MeV, 130.2 MeV, and 124.5 MeV: (a) depth dose distributions, (b) depth distributions of activity, (c) lateral dose distributions, (e) lateral distributions of activity.

mapped on a frame of 120.8×186.8 mm^2 every second. The detection counts per second were also stored in the data set. Moreover, the time-dependent changes and the differences between the PET images acquired in plans 1 and 2 were examined. In the case of this experiment, the internal organ motion effect and physiologic washout effect of the positron emitter nucleus[12] are not considered in the PET images.

III. RESULTS

A. Distributions of positron emitter nuclei generated in the water target

The measured distribution of positron emitter nuclei generated in the water target and the measured dose distribution were compared and verified. Figures 3(a) and 3(b) show the measured depth dose distributions and the measured depth distributions of positron emitter nuclei in the MONO proton beam at 135.8 MeV and fine degraded energies at 135.5 MeV (fine degrader: F.D.=0.0 mmWEL), 135.1 MeV (F.D.=1.2 mmWEL), 134.4 MeV (F.D.=2.3 mmWEL), 133.0 MeV (F.D.=4.6 mmWEL), 130.2 MeV (F.D. =9.3 mmWEL), and 124.5 MeV (F.D.=18.6 mmWEL), respectively. Similarly, Figs. 3(c) and 3(d) show the measured lateral distributions and the measured lateral distributions of the positron emitter nuclei.

Table I summarizes the measured physical range ($R_{\text{phy.}}$), the measured activity range ($R_{\text{act.}}$), which was defined as the depth point of the 50% peak of the activity, difference between their ranges (ΔR), each difference of physical and activity range against each range at 135.8 MeV ($\Delta R_{\text{phys.}}, \Delta R_{\text{act.}}$), and their differences ($\delta\Delta R$), in the water target irradiated with the proton MONO beams. Similarly, the beam center positions ($\text{BC}_{\text{dose}}, \text{BC}_{\text{act.}}$) of the dose and activity calculated by the measured lateral dose and activity distributions, and difference of each BC (ΔBC) are shown in Table I.

The ΔR obtained by the measurement results were about 1 mmWEL to 4 mmWEL. The threshold energy of the reaction calculated by difference of atomic weight is 16 MeV for the $^{16}\text{O}(p,pn)^{15}\text{O}$ reaction. The threshold energy of 16 MeV is estimated to be a range difference of about 3 mm WEL at the distal edge by the calculated result of a stopping power. The $\delta\Delta R$ were reproduced at an accuracy within a difference of less than 2 mmWEL in the energy levels. The measured activity range included a random error about ± 0.5 mm in the position of the target against the position of the BOLPs. The ΔBC were reproduced at an accuracy within a difference of less than 1 mmWEL. The values of the ΔR and the $\delta\Delta R$ were almost equal to the value of the positional resolution of the BOLPs.

B. Distributions of positron emitter nuclei generated in the rabbit

1. Changes of PET image according to measurement time

Figure 4 shows the calculated proton dose distribution and the measured PET images in the plan 1. The PET images

TABLE I. Differences between the measured physical range and the measured activity range in the water target irradiated with proton MONO at different energy levels.

Depth distribution	Fine degrader (F.D.) (mmWEL)	0	1.2	2.3	4.6	9.3	18.6
	$R_{\text{phys.}}$(F.D.) (mmWEL)	132.2	130.9	129.9	127.4	122.8	113.4
	R_{act}(F.D.) (mmWEL)	129.6	127.3	126.6	125.6	122.1	112.2
	$\Delta R_{\text{phys.}}$(F.D.) (mmWEL)[a]	···	1.3	2.3	4.8	9.5	18.9
	ΔR_{act}(F.D.) (mmWEL)[b]	···	2.3	3.0	4.0	7.5	17.4
	ΔR(F.D.) (mmWEL)[c]	2.6	3.6	3.3	1.8	0.7	1.1
	$\delta\Delta R$(F.D.) (mmWEL)[d]	···	−1.0	−0.6	0.8	1.9	1.5
Lateral distribution	BC_{dose} (mm)	0.0	1.0	1.9	4.0		
	BC_{act} (mm)	0.0	0.7	2.6	3.7		
	ΔBC[e](mm)	0.0	−0.2	0.6	−0.3		

[a] $\Delta R_{\text{phys.}}(\text{F.D.}) = R_{\text{phys.}}(0) - R_{\text{phys.}}(\text{F.D.})$
[b] $\Delta R_{\text{act}}(\text{F.D.}) = R_{\text{act}}(0) - R_{\text{act}}(\text{F.D.})$
[c] $\Delta R(\text{F.D.}) = R_{\text{phys.}}(\text{F.D.}) - R_{\text{act}}(\text{F.D.})$
[d] $\delta\Delta R(\text{F.D.}) = \Delta R_{\text{phys.}}(\text{F.D.}) - \Delta R_{\text{act}}(\text{F.D.})$
[e] $\Delta\text{BC} = \text{BC}_{\text{act}} - \text{BC}_{\text{dose}}$

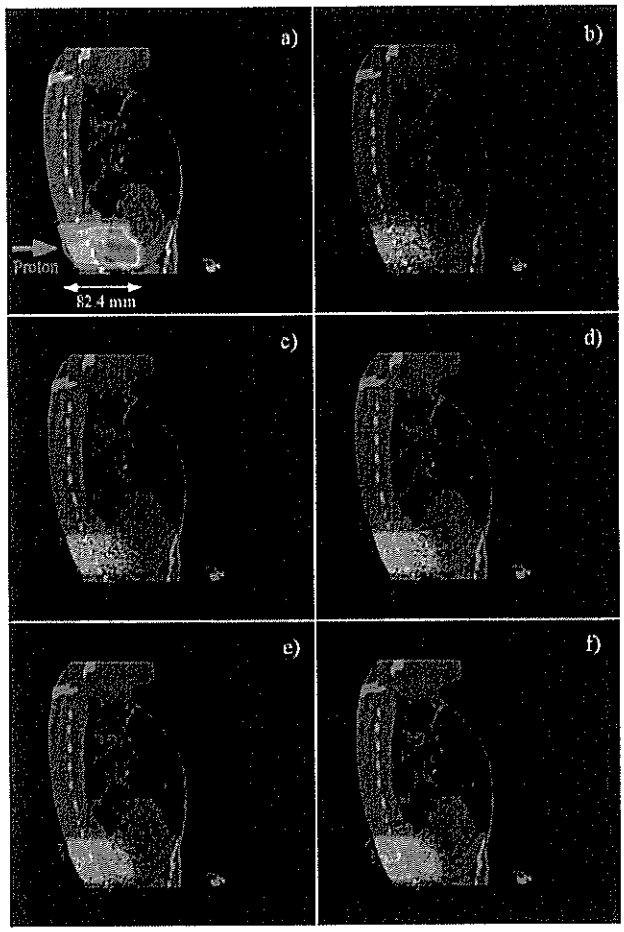

FIG. 4. Calculated proton dose distribution (a) and PET image measured at 1 (b), 2 (c), 4 (d), 10 (e), and 30 min (f) after proton irradiation in plan 1.

show the results of the measurements at 1, 2, 4, 10, and 30 min after the proton irradiation. Each number of total detection events was 114 583, 194 488, 295 555, 417 471, and 525 474 counts, respectively. The measured activity distribution corresponded to the irradiated dose distribution. The distinctness of the PET image increased as the time of the measurement using the BOLPs improved by increasing the detection events. However, further improvement of the distinctness of the PET image was not expected so that over 95% of the total detection events were collected by the measurement of 30 min. The detection counts per second of the activity generated in the rabbit is shown in Fig. 5. Moreover, a large amount of background data of the signal per noise ratio equal to about 1/10 among the proton irradiation, were included in the data collected from the measurement using the BOLPs. There are secondary x rays, gamma rays, and neutrons generated by the proton bombarding the device utilized for the formation of the irradiation field in the proton treatment. Therefore, the PET images were constructed by using only the detection events after the beam irradiation stop.

The generated positron emitter nuclei in the rabbit are

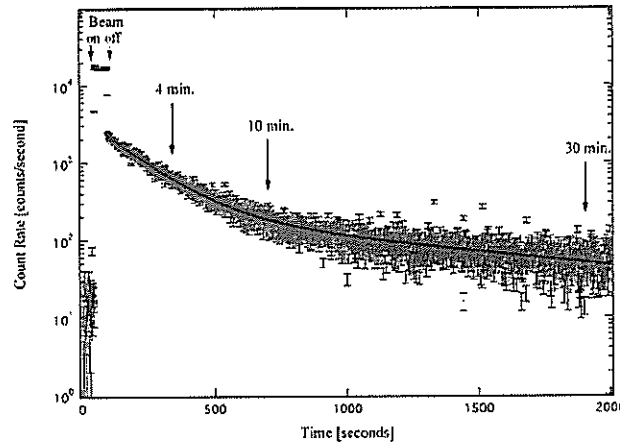

FIG. 5. Detection counts per second measured using the BOLPs in plan 1.

predicted to be mainly the ^{15}O, ^{14}O, ^{13}N, and ^{11}C nuclei. The decay of the activity was mainly ^{15}O for about 5 min after the proton irradiation, and ^{15}O, ^{13}N, and ^{11}C at times over 5 min. However, it is possible to approximate the function of the detection rate CR by dividing it into two elements with a short and long half-life time, as expressed by the following equations:

$$CR(t) = \sum_{i=^{15}O,^{14}O,^{13}N,^{11}C,\ldots} [CR(t)]_i$$

$$= \sum_{j=^{15}O,^{14}O,\ldots} [CR(t)]_j + \sum_{k=^{13}N,^{11}C,\ldots} [CR(t)]_k$$

$$\rightarrow 1977.9 \times \left(\frac{1}{2}\right)^{t/110.5} + 219.7 \times \left(\frac{1}{2}\right)^{t/847.6}. \quad (4)$$

Here, t denotes the measurement time, in second, after the beam stops.

2. Dependence of activity on maximum range

The results of the calculated dose distribution and the PET images acquired at 10 min using the BOLPs in plans 1 and 2 are shown in Fig. 6. In the calculated dose distribution, the maximum range was 82.4 mmWEL in plan 1, and 95.0 mmWEL in plan 2. The difference of the maximum range between plans 1 and 2 was 12.6 mmWEL. Both the measured activity distribution and the dose distribution in plan 2 reached a deeper point than those in plan 1. Figure 7 shows the depth profile of the activity distribution at 10 min measured using the BOLPs in plans 1 and 2. The differences between the activity range between plans 1 and 2 at the distal points of 3000 counts, 4000 counts, and 5000 counts were 14, 11, and 9 mm, respectively, as shown in Table II. The results showed a difference between the maximum range of 13 mmWEL.

IV. DISCUSSION AND CONCLUSIONS

In Japan, the proton treatment is generally performed with the daily fractional dose of 1.8–5.5 Gy and total dose of

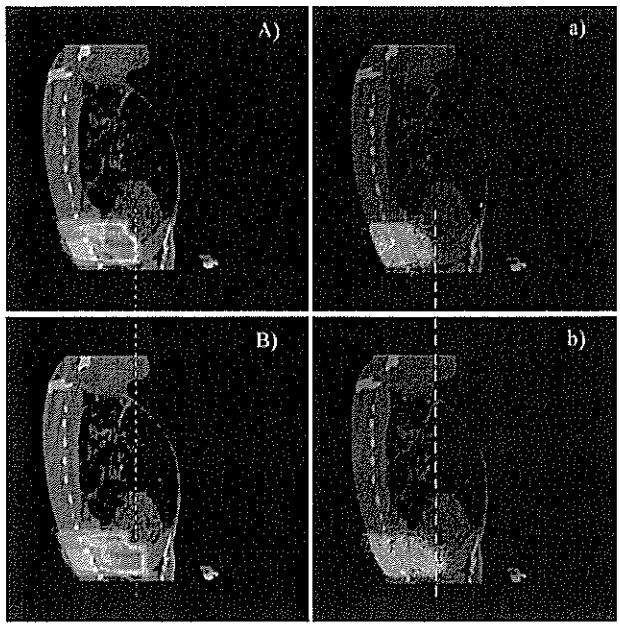

FIG. 6. Calculated proton dose distribution (A), (B) and PET images acquired at 10 min (a), (b) in plans 1 and 2, respectively.

59–73 Gy for each treatment site. The time period of the treatment is from 2 to 7 weeks. The proton treatment planning is done with 1–3 irradiation fields. One or two of the irradiation fields are used for a daily irradiation. During the period of proton treatment precise information about changes of the tumor and the patient condition are important as they pertain to the target volume position with respect to the beam. If a reduction of the tumor size occurs, a change of the body shape occurs during the comparatively long period of the treatment, and the treatment will be performed with a dose distribution different from the planned dose distribution. Figure 8 shows the dose distribution calculated for three field irradiation from the anterior direction and two noncoplanar directions in the case of a tumor of the paranasal

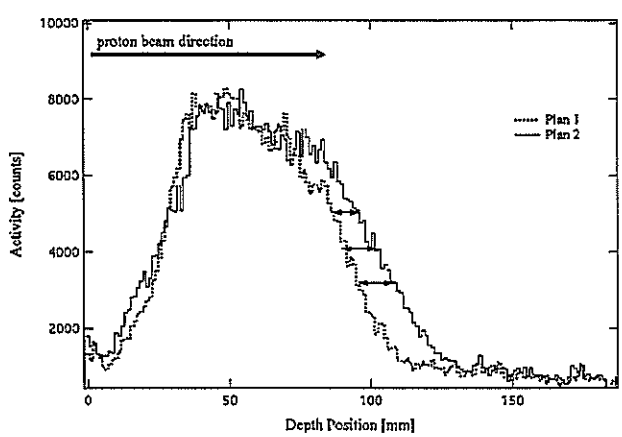

FIG. 7. Depth profile of the activity distribution in the measurement at 10 min using the BOLPs in plans 1 and 2, respectively.

TABLE II. Difference between the activity ranges in the plan 1 and 2 at each point of the distal activity.

Distal point activity: DPA (counts)	3000	4000	5000
Activity range: AR(Plan, DPA) (mm)			
Plan 1	97	93	89
Plan 2	111	104	98
AR(2.DPA)-AR(1.DPA) (mm)	14	11	9

sinuses. The irradiation dose is 59 Gy/26 fractions with one field irradiation/day. The left and right figures show the dose distribution immediately after beginning the treatment and after the partial reduction of the tumor in the air area of the paranasal sinuses, respectively. In the treatment plan, the dose is concentrated to the tumor and is low to the brain stem as the organ at risk. However, the concentration of the dose to the tumor is low, and a high dose is delivered to the brain stem due to the reduction of the tumor during the period of treatment.

In the experiment using the water target, the values of the $\delta\Delta R$ $(=\Delta R_{\text{phys.}}-\Delta R_{\text{act.}}=(R_{\text{phys.}}(0)-R_{\text{phys.}}(\text{F.D.}))-(R_{\text{act.}}(0)-R_{\text{act.}}(\text{F.D.})))$ and the ΔBC are a very important index for evaluation of the utility of the constructed BOLPs. The experimental results suggest that a change of the range of a few mmWEL, which is almost equal to the value of the positional resolution of the BOLPs, will be detected for the change of activity range measured using the BOLPs. The positional accuracy of an irradiated dose field will be under 1 mm by the values of the ΔBC. With the experimental results using the rabbit, the information needed for the analysis of the activity distribution will be obtained by the measurement at about 4 min after the proton irradiation with the daily fractional dose using a proton treatment. However, the number of 511-keV annihilation gamma rays will decrease in a patient. The attenuation length in water is about 10 cm. The half thickness of the rabbit's body in this experiment is about 5 cm WEL. Therefore, the number of gamma rays becomes about 175%–6% of the number in the experiment using the rabbit so that the pass length of a patient is about 2–20 cm WEL in a proton treatment. The effect of the attenuation in

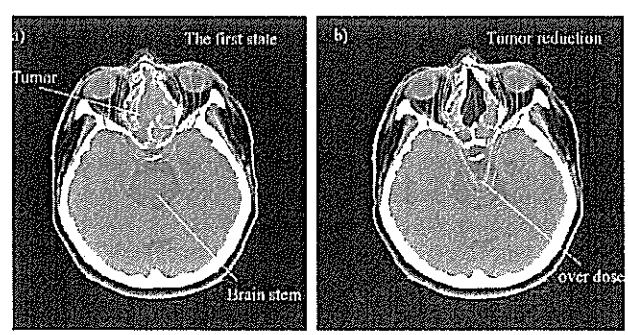

FIG. 8. Proton dose distribution of anterior direction and two noncoplanar directions in the case of a tumor of the paranasal sinuses calculated using the proton treatment planning system. The left figure shows the dose distribution immediately after the beginning of the treatment, and the right shows the dose distribution after partial reduction of the tumor.

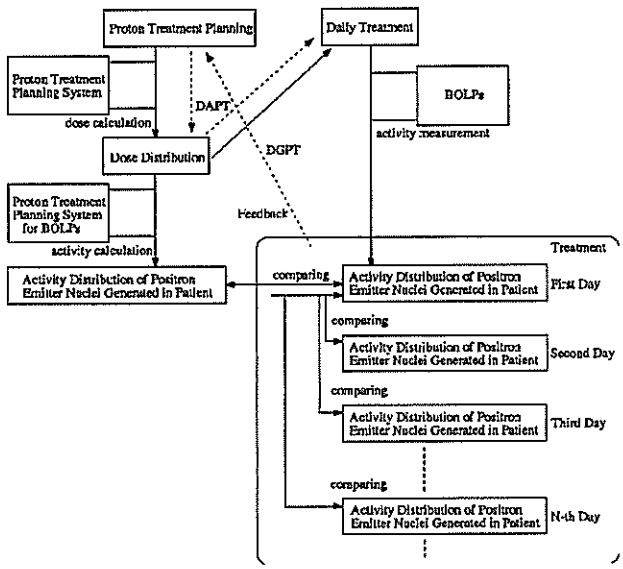

FIG. 9. Flow diagram of the procedure for the clinical use of the BOLPs.

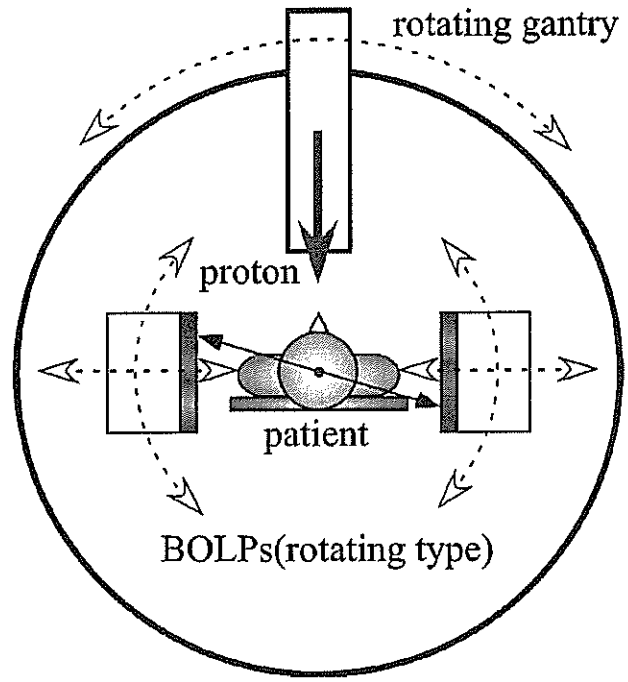

FIG. 10. View of the BOLPs equipped to rotate with the rotating gantry.

each patient will be necessary for the decision of the measurement time of the BOLPs. Another uncertainty in the future BOLPs application to human treatments is the effect of biologic isotope decay due to blood flow. The physiologic washout effect of the positron emitter nucleus that might be different by a body tissue was not considered in this experiment using the frozen rabbit. The activity distribution measured using the BOLPs will extend and become unclear by the effect. Therefore, the measurement in a short time will be important for a reduction of the effect. The difference in the physical range of 13 mm WEL was confirmed from the difference in the measured activity range in the rabbit. The results suggest that the proton treatment with high accuracy will be achieved by the DGPT using the BOLPs in the case shown in Fig. 8.

A flow chart of the DGPT in the proton treatment is shown in Fig. 9. The main operation is to take a PET image every day and compare the PET image of the first day of treatment with each PET image during the comparatively long period of treatment. Wherewith, if the difference between both images is confirmed by reducing the tumor size and changing the body shape, then the first proton treatment plan is immediately corrected to a new plan. As a result, proton treatments of high accuracy can be offered to the patient. In practice, the daily precision of the patient positioning and the irradiated beam condition will be evaluated with the change of the measured activity distribution. The change will be used for the setup of the margin in the proton treatment planning system. Moreover, the usefulness of this system will be high in spot scanning proton therapy and hypofractional proton therapy required for high irradiation accuracy. Especially, dose volume adapted proton therapy (DAPT), which can feed back to an optimum treatment on the spot, will be achieved as a high precision of the activity calculation in the DGPT using the BOLPs and a speed up of the dose calculation accurately in spot scanning proton therapy. On the other hand, the proton treatment has shifted to the treatment of a hypofractional dose and the new protocol is ongoing now.

The development of a BOLPs setup directly in the rotating gantry port shown in Fig. 10 is ongoing now. The distance of both the opposed detector arrays set up on the arms, which move to the parallel direction of a rotation axis and the direction of a gantry rotating, can be adjusted from 300 mm to 1000 mm. Also, the secondary x rays that are the main component of the background during the proton irradiation will be attenuated by the addition of a thin lead shield. As a result, the measurement of the activity using the BOLPs might become possible during proton irradiation.

ACKNOWLEDGMENTS

We would like to thank the staff members of the Proton Radiotherapy Department of the National Cancer Center, Kashiwa, for help, the members of the SHI Accelerator Service Ltd. and Accelerator Engineering Inc. for the operation of the proton apparatus, Dr. Y. Kurashima and Dr. H. Esumi of the National Cancer Center, Kashiwa, for the support and providing the rabbits for these experiments.

APPENDIX: DECAY CORRECTION OF ACTIVITY DURING PROTON IRRADIATION

Intensity of the proton beam provided from a cyclotron accelerator is almost constant. Therefore, the number of positron emitter nuclei N_R is expressed as follows:

$$N_R = \frac{dn}{dt} \cdot T_i, \quad \frac{dn}{dt} \approx \text{constant}. \tag{A1}$$

Here, dn/dt denotes a rate of number of positron emitter nuclei per time of beam irradiation. The residual number of positron emitter nuclei immediately after irradiation, N_{act}, can be expressed using Eq. (A1) by the following equations:

$$\begin{aligned}
N_{act} &= \frac{dn}{dt} \cdot \Delta t \cdot \exp\left(-\frac{\ln 2}{T_{1/2}} \cdot \Delta t \cdot m\right) \\
&\quad + \frac{dn}{dt} \cdot \Delta t \cdot \exp\left(-\frac{\ln 2}{T_{1/2}} \cdot \Delta t \cdot (m-1)\right) + \cdots \\
&\quad + \frac{dn}{dt} \cdot \Delta t \cdot \exp\left(-\frac{\ln 2}{T_{1/2}} \cdot \Delta t \cdot 0\right) \\
&= \sum_{m=0}^{l} \frac{dn}{dt} \cdot \Delta t \cdot \exp\left(-\frac{\ln 2}{T_{1/2}} \cdot \Delta t \cdot m\right) \\
&\quad \text{(where } l,m = \text{sample number)} \\
&= \sum_{t'=0}^{T_i} \frac{dn}{dt} \cdot \frac{t'}{m} \cdot \exp\left(-\frac{\ln 2}{T_{1/2}} \cdot t'\right) \\
&\quad \text{(where } \Delta t \cdot l = T_i, \Delta t \cdot m = t') \\
&\to \int_0^{T_i} \frac{dn}{dt} \cdot \exp\left(-\frac{\ln 2}{T_{1/2}} \cdot t'\right) dt' \quad (\text{as } m \to \infty, \Delta t \to 0) \\
&= \frac{dn}{dt} \cdot \frac{T_{1/2}}{\ln 2} \cdot \left[\exp\left(-\frac{\ln 2}{T_{1/2}} \cdot t'\right)\right]_{T_i}^{0} \\
&= \frac{dn}{dt} \cdot \frac{T_{1/2}}{\ln 2} \cdot (1 - 2^{-T_i/T_{1/2}}) \\
&= N_R \cdot \frac{T_{1/2}}{T_i \cdot \ln 2} \cdot (1 - 2^{-T_i/T_{1/2}}).
\end{aligned} \tag{A2}$$

Here, if

$T_{1/2} \gg T_i$:

$$\begin{aligned}
N_{act} &\approx N_R \cdot \frac{T_{1/2}}{T_i \cdot \ln 2} \cdot \left(1 - \left(1 - \frac{\ln 2}{T_{1/2}} \cdot T_i\right)\right) \\
&= N_R \cdot \frac{T_{1/2}}{T_i \cdot \ln 2} \cdot \frac{\ln 2}{T_{1/2}} \cdot T_i = N_R.
\end{aligned} \tag{A3}$$

And, if

$$T_{1/2} \ll T_i; \quad N_{act} \approx N_R \cdot \frac{T_{1/2}}{T_i \cdot \ln 2} = \frac{dn}{dt} \cdot \frac{T_{1/2}}{\ln 2} = \text{constant}. \tag{A4}$$

[a]Electronic mail: tnishio@east.ncc.go.jp

[1]PARTICLES 34 PTCOG Newsletter, July, 2004.
[2]R. G. Simpson, C. T. Chen, E. A. Grubbs, and W. Swindell, "A 4-MV scanner for radiation therapy: The prototype system," Med. Phys. 9(4), 574–579 (1982).
[3]K. Nakagawa, Y. Aoki, K. Sakata, K. Karasawa, N. Muta, K. Kojima, Y. Onogi, Y. Hosoi, A. Akanuma, and M. Ito, "Dynamic therapy utilizing CT-Linac on line system," Proceedings of the 9th ICCRT, 1987, pp. 541–544.
[4]T. Nishio, T. Sato, H. Kitamura, K. Murakami, and T. Ogino, "Distributions of β^+ decayed nuclei generated in the CH_2 and H_2O targets by the target nuclear fragment reaction using therapeutic MONO and SOBP proton beam," Med. Phys. 32(4), 1070–1082 (2005).
[5]K. Parodi, W. Enghardt, and T. Haberer, "In-beam PET measurements of β^+ radioactivity induced by proton beams," Phys. Med. Biol. 47, 21–36 (2002).
[6]D. W. Litzenberg, D. A. Roberts, M. Y. Lee, K. Pham, A. M. Vander Molen, R. Ronningen, and F. D. Becchetti, "On-line monitoring of radiotherapy beams: Experimental results with proton beams," Med. Phys. 26(6), 992–1006 (1999).
[7]"ICRU Report 46: Photon, Electron, Proton and Neutron Interaction Data for Body Tissues," ICRU, 1992, pp. 11–13.
[8]H. Uchida, T. Okamoto, T. Ohmura, K. Shimizu, N. Satoh, T. Koike, and T. Yamashita, "A compact planar positron imaging system," Nucl. Instrum. Methods Phys. Res. A 516, 564–574 (2004).
[9]T. Nishio, "Proton therapy facility at National Cancer Center, Kashiwa, Japan," J. At. Energy Soc. 41(11), 1134–1138 (1999).
[10]T. Nishio, T. Ogino, M. Sakudo, N. Tanizaki, M. Yamada, G. Nishida, H. Nishimura, and H. Ikeda, "Present proton treatment planning system at National Cancer Center Hospital East," Jpn. J. Med. Phys. Proc. JSMP2000 20, Suppl. 4, 174–177 (2000).
[11]T. Nishio, K. Suegara, M. Yamada, and T. Ogino, "Construction of the proton treatment planning system possessing high versatility and development environment," Jpn. J. Med. Phys. Proc. JSMP2003 23, Suppl. 3, 67–68 (2003).
[12]H. Mizuno, T. Tomitani, M. Kanazawa, A. Kitagawa, J. Pawelke, Y. Iseki, E. Urakabe, M. Suda, A. Kawano, R. Iritani, S. Matsushita, I. Inaniwa, T. Nishio, S. Furukawa, K. Ando, Y. K. Nakamura, T. Kanai, and K. Ishii, "Washout measurement of radioisotope implanted by radioactive beam in the rabbit," Phys. Med. Biol. 48, 2269–2281 (2003).

J Cancer Res Clin Oncol
DOI 10.1007/s00432-006-0168-7

ORIGINAL PAPER

Changes in pelvic and systemic platinum concentrations during negative-balance isolated pelvic perfusion: correlation between platinum concentration and method of administration in a pig model

Satoru Murata · Hiroyuki Tajima · Yutaka Abe · Shiro Onozawa · Fumio Uchiyama · Hiromitsu Hayashi · Ryoji Kimata · Kazuhiro Nomura

Received: 12 April 2006 / Revised: 7 June 2006 / Accepted: 1 November 2006

Abstract
Purpose To assess the effect of altering the method of administration during negative-balance isolated pelvic perfusion (NIPP) on the platinum concentration in the pelvic or systemic circulation.
Methods Twenty female pigs were used in this study. The abdominal aorta and the infra-renal vena cava were occluded with two balloon catheters and blood in the extracorporeal circuit was circulated with twin rotary pumps. NIPP was then performed with cisplatin (5 mg/kg) in 15 pigs. Three types of NIPP administration method (group A: 1 bolus, B: 2 same doses boluses, C: 3 same doses boluses) were used, five pigs being subjected to each treatment. The remaining five pigs were administered cisplatin systemically as a control study (group D). The platinum concentrations in the pelvic and systemic circulation were measured and compared.
Results (1) Pelvic circulation: There was a tendency for the platinum concentration to increase as the bolus time decreased. The platinum concentration in groups A and B was significantly ($P < 0.05$) higher than that in group C. Significant differences ($P < 0.05$) between groups A and B until 10 min after the start of NIPP. (2) Systemic circulation: Significant differences ($P < 0.05$) were observed between NIPP groups and D during NIPP. The platinum concentration in group D was five times higher than that in group C. (3) Plasma pelvic to systemic exposure ratio: there were no significant differences among the three NIPP groups.
Conclusions The platinum concentrations in the pelvic and systemic circulation increased as the bolus time decreased. The plasma pelvic to systemic exposure ratio was not influenced by bolus time.

Keywords Isolated pelvic perfusion · Negative-balance isolated pelvic perfusion · Pig model

S. Murata (✉) · H. Tajima · Y. Abe · S. Onozawa · F. Uchiyama · H. Hayashi
Department of Radiology, Center for Advanced Medical Technology, Nippon Medical School, 1-1-5 Sendagi, Bunkyou-ku, Tokyo 113-8602, Japan
e-mail: genji@nms.ac.jp

R. Kimata
Department of Urology, Nippon Medical School, 1-1-5 Sendagi, Bunkyou-ku, Tokyo 113-8602, Japan

K. Nomura
National Cancer Center Hospital, 5-1-1 Tsukiji, Chuo-ku, Tokyo 104-0045, Japan

Introduction

During the last four or five decades, there have been many attempts to enhance tumor response by isolated pelvic perfusion (IPP) therapy in which anticancer drugs at high concentrations are delivered to the tumor tissue as selectively as possible. The first regional perfusion technique, initiated by Creech et al. (1958), was the use of an extracorporeal circuit to deliver a high concentration of drug to a regional arterial/venous circuit in an extremity. IPP was first developed by Austen et al. (1959) and has been used by several medical groups in an effort to control advanced malignancies of the bladder, uterus and rectum (Austen et al. 1959; Watkins et al. 1960; Stehlin et al. 1960; Shingleton et al. 1961; Lawrence et al. 1961, 1963; Collins 1989; Wile and Smolin 1987; Wile et al. 1985; Turk et al. 1993;

Wanebo and Belliveau 1999; Wanebo et al. 1996, 2003; Guadagni et al. 1998). However, IPP therapy has not been used as a therapeutic strategy for advanced pelvic cancers. Even in an isolated setting, anticancer agents can easily leak into the systemic circulation (Lawrence et al. 1961, 1963; Wile and Smolin 1987; Wile et al. 1985; Collins 1989; Turk et al. 1993; Wanebo and Belliveau 1999; Wanebo et al. 1996, 2003). Therefore, it is impossible to perform such therapy in patients with renal dysfunction and the amount of anti-cancer agents is strictly limited.

We hypothesized that drug leakage via highly developed collateral vessels in the pelvis into the systemic circulation would be decreased by reducing the blood pressure in the pelvic venous circulation during IPP and for this purpose we developed a twin-pump system for the extracorporeal circuit to modulate the in–out flow rate in an IPP pig model (Murata et al. 2005). We devised a novel IPP technique that allowed control of a negative-balance in–out flow rate, which we refer to as negative-balance isolated pelvic perfusion (NIPP) and found that this clearly reduced drug leakage into the systemic circulation. In the present study, in order to determine the most appropriate method of administration, we evaluated the contribution of drug administration time to platinum concentration in the pelvic and systemic circulation in a pig model.

Materials and methods

Animal model and general anesthesia

All animal experiments were conducted in accordance with the Guidelines of Nippon Medical School University for Animal Care and Experimentation. Twenty adult female pigs weighing 34–40 kg (average: 36 kg) were used in this study and all procedures were performed with the animals under general anesthesia. The animals were placed supine and general anesthesia was induced with an intramuscular injection of ketamine hydrochloride (300 mg/pig) and maintained with sevoflurane (Maruishi Pharmaceutical Co. Ltd., Osaka, Japan).

Monitoring of the systemic circulation

Peripheral arterial oxygen saturation was maintained above 90% and monitored with a probe applied to the ear. Each animal was continuously monitored during the procedure using electrocardiography. In all 20 pigs, both internal jugular veins were exposed through a cut-down incision and two cannula sheaths (5 Fr; Medikit Co. Ltd. Japan) were inserted into each of them. The cannula sheath in the right jugular vein was used to collect blood samples and to monitor central venous pressure (CVP) and the other sheath was used to administrate other agents by intravenous drip infusion. The thyrocervical artery was exposed and a 5 Fr cannula sheath was inserted to monitor blood pressure during the procedures. CVP and arterial blood pressure were recorded before and at 0, 5, 10, 15, 20, 25 and 30 min after the start of perfusion.

Catheter technique and experimental groups

Additional procedures were performed in 15 pigs subjected to NIPP. Both common femoral arteries and veins were exposed through a cut-down incision and sheaths (6 and 9 Fr each; Medikit Co. Ltd., Tokyo, Japan) were inserted into each of them, as shown in Fig. 1 (Murata et al. 2005). The cannulas had specially designed side-arms to allow high flow and to keep the pressure in the pump-system low during withdrawal and return of the blood through the cannulas. After systemic heparinization (120 U/kg), two balloon catheters (30 mm balloon with 5 Fr shaft, Forte Co. Ltd., Tokyo, Japan) were placed in the abdominal aorta and the infrarenal vena cava (IVC) at the level of the L3/4 intervertebral space.

Among the 20 pigs, 15 were evaluated for the contribution of drug administration time to platinum concentration in the pelvic and systemic circulation by using three sets of bolus infusions. After occlusion of the abdominal aorta and IVC with the two balloon catheters, blood was withdrawn from the veins with one of the rotary pumps and returned to the arteries through the cannulas with the other rotary pump. Five animals were allocated to each group; a total cisplatin (Nippon Kayaku Co. Ltd., Tokyo, Japan) dose of 5 mg/kg was

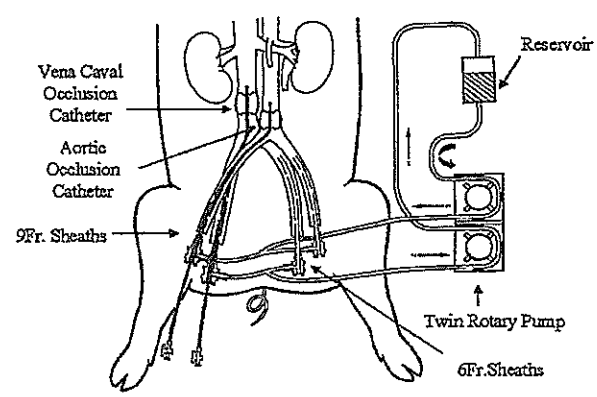

Fig. 1 Schema of the negative-balance isolated pelvic perfusion system used in a pig model (Murata et al. 2005)

administered into the reservoir (Fig. 1) in one bolus (group A), in two equal boluses at 0 and 10 min after the beginning of perfusion (group B), or in three equal boluses at 0, 10 and 20 min after the beginning of perfusion (group C). The volume withdrawn was fixed of 20 ml/min higher than the volume returned (300 ml/min). The remaining five pigs (group D) were subjected to systemic intravenous administration of cisplatin in three equal boluses as a control study. In this group, cisplatin was administered for 1 min per bolus. The reason why we used much higher dose of cisplatin than that used with humans was to obtain a data of blood kinetics of high cisplatin dose for clinical application because there were very few papers with double or triple doses of cisplatin.

Management of systemic circulation

The animals were administered the other agents by intravenous drip infusion via the cannula sheath in the left jugular vein during IPP, because the reduction of blood volume caused by increasing the volume withdrawn and the volume of the blood samples would have caused anemia in the pigs. In view of the volume of blood loss during NIPP, the intravenous drip infusion rate was set at 25 ml/min in each group. The cisplatin was infused for 30 min. In group D, the intravenous drip infusion rate was set at 5 ml/min. All results were performed independently five times.

Angiography

Before NIPP, isolated pelvic angiography was performed with the twin rotary pumps in each animal ($n = 15$) to confirm establishment of the IPP system. Isolated pelvic angiography was performed by infusion of non-ionic contrast material (300 mg/ml; iodine, iohexol, Daiichi Pharmaceutical Co. Ltd., Japan) at a rate of 5 ml/s through the arteries with a rotary pump and was withdrawn at a rate of 5 ml/s through the veins with the other rotary pump. The duration of angiography was 30 s and the total volume of contrast material infused was 100 ml. Recording of the fluoroscopic images on video tape was begun at the start of contrast material infusion. NIPP was performed after confirming that no contrast material had entered the inferior vena cava above the occluding balloon.

Analysis of pharmacokinetics

In NIPP groups, plasma platinum concentration was measured in blood samples collected from the arterial and venous sides of the pump and from the systemic venous circulation (superior vena cava) at 0, 5, 10, 15, 20, 25 and 30 min after the start of NIPP. Blood samples in groups B and C were collected 10 and 20 min prior to the second or third injection of cisplatin. In group D, the plasma platinum concentration was also measured in blood samples collected from the systemic venous circulation (superior vena cava) at 0, 5, 10, 15, 20, 25 and 30 min after the start of cisplatin infusion. Blood samples in group D were collected 10 and 20 min prior to the second or third injection of cisplatin.

Statistical analysis

The plasma samples were digested with nitric acid for analysis of metal species. Platinum concentrations in the serum were measured by atomic absorption spectrophotometry (Varian SpectrAA 300/400). Drug exposure was measured as the area under the serum concentration–time curve until 30 min after the start of perfusion. All data are shown as means ± SD. Results were compared by ANOVA with repeated measures and Games–Howel method as post hoc comparisons. Differences at $P < 0.05$ were considered statistically significant.

Results

Effect of NIPP on the systemic circulation

Hemodynamic parameters, arterial blood pressure (BP), heart rate (HR), blood oxygen saturation (SAT) and CVP were measured during NIPP to evaluate its effect on the systemic circulation. Each animal was hemodynamically stable throughout all the procedures.

Pharmacokinetics of the serum platinum concentration in the pelvic circulation

Serum plasma platinum .concentrations in the pelvic circulation

The maximum plasma platinum concentrations in the pelvic circulation on the arterial side (Table 1; Fig. 2) were 75.0 (15.5) mg/l in group A, 55.8 (7.3) mg/l in group B and 38.2 (5.6) mg/l in group C. The average platinum concentration was 43.6 (9.0) mg/l in group A, 37.9 (2.0) mg/l in group B and 28.3 (1.6) mg/l in group C. The maximum plasma platinum concentrations in the pelvic circulation on the venous side (Table 1; Fig. 3) were 59.7 (15.8) mg/l in group A, 38.9 (7.4) mg/l in group B and 29.2 (4.3) mg/l in group C. The average